

AD-A080 849

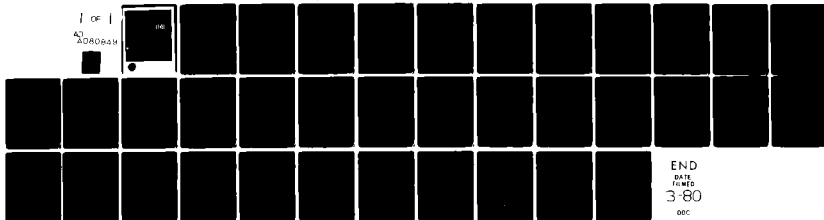
ARIZONA UNIV TUCSON INST OF ATMOSPHERIC PHYSICS
DUAL-FREQUENCY DOPPLER-LIDAR METHOD OF WIND MEASUREMENT.(U) F/6 14/2
JAN 80 W L EBERHARD, R M SCHOTLAND DAA629-76-8-0115

UNCLASSIFIED

ARO-13343.1-65

NL

1 OF 1
AD A080849



END
DATE
FORWED
3-80
DDC

DDC FILE COPY

ADA 080849

(6) DUAL-FREQUENCY DOPPLER-LIDAR METHOD OF WIND MEASUREMENT.

(9) FINAL REPORT. 1 Dec 75 - 30 Nov 79, 12

(10) Wynn L. Eberhard Richard M. Schotland

(11) 22 Jan 80

LEVEL

(12) 37 U. S. ARMY RESEARCH OFFICE

(15) Grants DAAG29-76-G-0115, and DAAG29-79-G-0026

DDC
RECEIVED
FEB 14 1980
E

(14) 1
Institute of Atmospheric Physics,
University of Arizona
Tucson, Arizona 85721

(13) ARD (19) 12375.1-GS
*Now with NOAA/ERL Wave Propagation Laboratory, Boulder, CO 80302

Approved for Public Release; Distribution Unlimited.

The findings in this report are not to be construed as an official department of the Army position, unless so designated by other authorized documents.

180800

Unclassified

SECURITY CLASSIFICATION OF THIS PAGE (When Data Entered)

REPORT DOCUMENTATION PAGE		READ INSTRUCTIONS BEFORE COMPLETING FORM
1. REPORT NUMBER 1	2. GOVT ACCESSION NO.	3. RECIPIENT'S CATALOG NUMBER
4. TITLE (and Subtitle) DUAL-FREQUENCY DOPPLER-LIDAR METHOD OF WIND MEASUREMENT		5. TYPE OF REPORT & PERIOD COVERED Final 12/1/75-11/30/79
7. AUTHOR(s) Wynn L. Eberhard, NOAA/ERL Wave Propagation Laboratory, Boulder, CO 80302 Richard M. Schotland		6. PERFORMING ORG. REPORT NUMBER
9. PERFORMING ORGANIZATION NAME AND ADDRESS Institute of Atmospheric Physics University of Arizona Tucson, Arizona 85721		8. CONTRACT OR GRANT NUMBER(s) DAAG29-76-G-0115 ⁴² DAAG29-79-G-0026
11. CONTROLLING OFFICE NAME AND ADDRESS U. S. Army Research Office Post Office Box 12211 Research Triangle Park, NC 27709		10. PROGRAM ELEMENT, PROJECT, TASK AREA & WORK UNIT NUMBERS
14. MONITORING AGENCY NAME & ADDRESS (if different from Controlling Office) Geosciences Division U.S. Army Research Office Box CM, Duke Station Durham, North Carolina 27706		12. REPORT DATE January 22, 1980
		13. NUMBER OF PAGES 35
		15. SECURITY CLASS. (of this report) Unclassified
		15a. DECLASSIFICATION/DOWNGRADING SCHEDULE NA
16. DISTRIBUTION STATEMENT (of this Report) Approved for public release; distribution unlimited.		
17. DISTRIBUTION STATEMENT (of the abstract entered in Block 20, if different from Report) NA		
18. SUPPLEMENTARY NOTES The findings in this report are not to be construed as an official Department of the Army position, unless so designated by other authorized documents.		
19. KEY WORDS (Continue on reverse side if necessary and identify by block number) Lidar, Winds, Laser, Doppler		
20. ABSTRACT (Continue on reverse side if necessary and identify by block number) In this new method (DFDL) of remote wind sensing, two optical beams of unlike frequency are superimposed in the sensed volume. The velocity information is obtained from the difference in the Doppler shifts of light scattered from the two beams by aerosols moving with the air. The DFDL signal spectrum and expressions for signal-to-noise ratio are derived. Attractive characteristics of DFDL include resilience to optical imperfections of the turbulent atmosphere and a potential for simultaneous measurement of the three components of wind velocity.		

DD FORM 1 JAN 73 1473

EDITION OF 1 NOV 65 IS OBSOLETE

Unclassified

SECURITY CLASSIFICATION OF THIS PAGE (When Data Entered)


Table of Contents

Page No.


- 2. Abstract
- 3. I. Introduction
- 4-17. II. Theory
- 17-19. III. Prototype DFDL
- 19-23. IV. Wind Measurements
 - 21. Table I. Summary of Selected Wind Data Runs
- 23-26. V. Projected Capabilities
- 26-27. VI. Summary
- 28. References
- 29. Figure Legends
- 30-34. Figures 1 thru 5
- 35. List of all publications and technical reports published, and a list of all participating scientific personnel showing advanced degree earned while employed on this project.

Accession For	
NTIS GRA&I	<input checked="checked" type="checkbox"/>
DDC TAB	<input type="checkbox"/>
Unannounced	<input type="checkbox"/>
Justification	
By _____	
Distribution/ _____	
Availability Codes	
Dist	Avail and/or special
A	

ABSTRACT



In this new method (DFDL) of remote wind sensing, two optical beams of unlike frequency are superimposed in the sensed volume. The velocity information is obtained from the difference in the Doppler shifts of light scattered from the two beams by aerosols moving with the air. The DFDL signal spectrum and expressions for signal-to-noise ratio are derived. Attractive characteristics of DFDL include resilience to optical imperfections of the turbulent atmosphere and a potential for simultaneous measurement of the three components of wind velocity.



I. Introduction

Several techniques for laser remote sensing of wind velocity have been experimentally demonstrated.¹⁻⁷ Unlike *in situ* devices, remote wind sensors avoid the necessity for providing an instrument-mounting platform that can reach the sampled points, and they do not perturb the air flow. Each laser technique possesses its own set of attributes that determine its usefulness for various applications. For instance, the heterodyne laser Doppler velocimeter,^{1,2} commonly using a CO₂ laser operating at 10.6 μm , determines the component of velocity parallel to the beam. The same component is found by the optical Doppler radar,³ which uses a scanning Fabry-Perot interferometer. The dual-beam Doppler anemometer⁴ and time-of-flight laser anemometer⁵ measure the component of wind along a direction transverse to the probing beams and perform best with lasers operating in the visible. These four techniques depend on aerosols as tracer targets of air motion. Two other techniques^{6,7} sense the motion of spatial inhomogeneities of the aerosol distribution in the atmosphere as they are transported by the wind. The full list of important characteristics for each technique, such as range capability and spatial resolution, is too lengthy to give here. Although the several techniques possess some similarities, their performance capabilities, which determine their utility in a particular application, are substantially different.

Dual-frequency Doppler-lidar (DFDL) is a new technique with a unique set of attributes that could make it the preferred sensor in some applications. In DFDL, two laser beams of unlike frequencies, ν_1 and ν_2 , where the frequency difference

$$\alpha = \nu_1 - \nu_2 \quad (1)$$

is in the microwave region, are transmitted to the probed volume. Light scattered to a photodetector by aerosols moving with the air is Doppler-shifted in frequency. Since the magnitude of the frequency shift depends not only on the aerosol's velocity, but also on both the frequency of the incident radiation and the scattering angle, there exists a difference, $\Delta\lambda$, between the Doppler shifts, $\Delta\nu_1$ and $\Delta\nu_2$. Electronic processing of the output of the square-law photodetector yields the differential Doppler shift, $\Delta\lambda$, and hence a component of wind velocity in the probed volume. The direction of this measured component depends on whether the two beams are exactly superimposed and parallel (pure DFEL) or intersect with small angular separation in the probed volume (hybrid DFEL). In this report, we derive the DFEL signal and describe how to extract the appropriate velocity component from the signal. An experimental DFEL system was constructed for the purpose of verifying the DFEL principle and evaluating the practical potential of this method for remote wind sensing using naturally existing aerosols as tracers. This device is briefly described and its successful performance reported.

II. Theory

A. Signal Derivation (Pure DFEL)

The signal for the pure DFEL case will be derived with reference to Fig. 1. Two optical beams of frequencies ν_1 and ν_2 , plane polarized in the same direction, are superimposed, with both traveling in the \hat{a} -direction to illuminate a volume containing air molecules and aerosols. The amplitude of the radiation transmitted to the i th particle, located at \vec{R}_i , can be expressed as

$$\vec{E}' = A_1 \cos(\omega_1 t - \vec{k}_1 \cdot \vec{R}_i) + A_2 \cos(\omega_2 t - \vec{k}_2 \cdot \vec{R}_i), \quad (1)$$

where the wave vectors \vec{k}_1 and \vec{k}_2 are parallel. The arbitrary phases of both frequencies in Eq. (2) have been taken as zero, a simplification which does not alter the final results. The amplitudes A_1 and A_2 are normalized, so that the irradiance is given by

$$M' = 2 \langle E'^2 \rangle_{\nu}, \quad (3)$$

where $\langle \rangle_{\nu}$ denotes a time average over optical frequencies but not over frequencies in the microwave region near α and below. Defining

$$\vec{K} = \vec{k}_1 - \vec{k}_2, \quad (4)$$

where $K = \alpha/c$, and c is the speed of light, the irradiance at a particle is

$$M' = A_1^2 + A_2^2 + 2A_1A_2 \cos(\alpha t - \vec{K} \cdot \vec{R}_p). \quad (5)$$

The transmitted irradiance is modulated at frequency α because the two beams interfere temporally to form a pattern of sinusoidal fringes which travel at the speed of light in the z -direction with an orientation normal to the z -axis. The fringe spacing is $\lambda_p = 2\pi/K$, and \vec{K} can be considered an effective wave vector for the traveling fringe pattern.

The molecules and aerosols scatter light from both beams to a point \vec{R}_d on a distant detector aperture. Assuming a particle's angular scatter cross section, $\sigma_i = S_i^2$, to be equal for ν_1 and ν_2 , and defining

$$\vec{L}_i = \vec{R}_{di} - \vec{R}_p, \quad (6)$$

the received radiation field at \vec{R}_d is

$$\begin{aligned} E &= \sum_i E_i \\ &= \sum_i (S_i / r_i^2) \left[A_1 \cos(\omega_1 t - \vec{k}_1 \cdot \vec{R}_p - \vec{k}_{1i} \cdot \vec{L}_i) \right. \\ &\quad \left. + A_2 \cos(\omega_2 t - \vec{k}_2 \cdot \vec{R}_p - \vec{k}_{2i} \cdot \vec{L}_i) \right], \end{aligned} \quad (7)$$

where the summation is over all particles scattering energy to \vec{R}_d . For non-relativistic particle speeds, the wave vector of radiation scattered from beam #1 is closely approximated by

$$\vec{k}_{1i} = k_1 \vec{L}_i / L_i, \quad (8)$$

with a similar expression existing for \vec{k}_{2i} .

The output current, I , of the photodetector is proportional to the received irradiance integrated over the aperture area, A_d , namely

$$I = \mathcal{R} \iint_{A_d} \langle E^2 \rangle_v dA_d, \quad (9)$$

where detector responsivity is assumed constant over the aperture. The detector will respond to modulation of the received irradiance within the limits of its electronic bandwidth. Equivalently, since a photodetector is a square-law device and if the received optical radiation contains two frequencies, a beat signal oscillating at the optical frequency difference is present in the output. We have

$$\begin{aligned} \langle E^2 \rangle_v &= \left\langle \sum_i \sum_j E_i E_j \right\rangle_v \\ &= \frac{1}{2} \sum_i \sum_j \frac{S_i S_j}{L_i L_j} \left[A_1^2 \cos[\vec{k}_1 \cdot (\vec{R}_i - \vec{R}_j) + \vec{k}_{1i} \cdot \vec{L}_i - \vec{k}_{1j} \cdot \vec{L}_j] \right. \\ &\quad + A_2^2 \cos[\vec{k}_2 \cdot (\vec{R}_i - \vec{R}_j) + \vec{k}_{2i} \cdot \vec{L}_i - \vec{k}_{2j} \cdot \vec{L}_j] \\ &\quad \left. + 2A_1 A_2 \cos[\omega t - \vec{k}_1 \cdot \vec{R}_i + \vec{k}_2 \cdot \vec{R}_j - \vec{k}_{1i} \cdot \vec{L}_i + \vec{k}_{2j} \cdot \vec{L}_j] \right]. \end{aligned} \quad (10)$$

Defining the effective wave vector for the scattered fringes as

$$\vec{K}_i = \vec{k}_{1i} - \vec{k}_{2i} \quad (11)$$

and separating the terms in the summation for which $i = j$ from the remainder,

$$\begin{aligned}
 \langle E^2 \rangle_v &= \frac{1}{2} \sum_i (S_i^2/L_i^2) (A_1^2 + A_2^2) \\
 &+ \sum_i (S_i^2/L_i^2) A_1 A_2 \cos[\omega t - \vec{k} \cdot \vec{R}_i - \vec{k}_i \cdot \vec{L}_i] \\
 &+ \frac{1}{2} \sum_i \sum_{j \neq i} \frac{S_i S_j}{L_i L_j} \left[A_1^2 \cos[\vec{k}_1 \cdot (\vec{R}_i - \vec{R}_j) + \vec{k}_{1i} \cdot \vec{L}_i - \vec{k}_{1j} \cdot \vec{L}_j] \right. \\
 &\quad \left. + A_2^2 \cos[\vec{k}_2 \cdot (\vec{R}_i - \vec{R}_j) + \vec{k}_{2i} \cdot \vec{L}_i - \vec{k}_{2j} \cdot \vec{L}_j] \right. \\
 &\quad \left. + 2A_1 A_2 \cos[\omega t - \vec{k}_1 \cdot \vec{R}_i + \vec{k}_2 \cdot \vec{R}_j - \vec{k}_{1i} \cdot \vec{L}_i + \vec{k}_{2j} \cdot \vec{L}_j] \right]. \quad (12)
 \end{aligned}$$

Let us first consider a single particle within the dual-frequency beam and later return to the multi-particle case. For one particle traveling with constant velocity \vec{V}_i , so that $\vec{R} = \vec{R}_{0i} + \vec{V}_i t$, Eq. (12) reduces to

$$\langle E_i^2 \rangle = \frac{1}{2} \frac{S_i^2}{L_i^2} \left[A_1^2 + A_2^2 + 2A_1 A_2 \cos[\omega t - (\vec{k} - \vec{k}_i) \cdot \vec{V}_i t - \vec{k}_i \cdot \vec{R}_{0i} + \phi_i] \right], \quad (13)$$

where $\phi_i = (\vec{k} - \vec{k}_i) \cdot \vec{R}_{0i}$ is the phase determined by particle position at $t = 0$. The DC terms A_1^2 and A_2^2 contain no Doppler information. The differential Doppler shift is

$$\Delta\omega = -(\vec{k} - \vec{k}_i) \cdot \vec{V} = -2K \sin(\theta/2) V_{\parallel}, \quad (14)$$

where θ is the scattering angle and V_{\parallel} is the component of \vec{V} parallel to the bisector of the transmitted and scattered directions. From the fringe viewpoint, the rate of arrival of the scattered fringes is altered by $\Delta\omega$ because the optical path length changes according to the particle's motion. For backscatter ($\theta = 180^\circ$), V_{\parallel} is the longitudinal velocity component (parallel to the direction of beam propagation). Through the differential Doppler

shift, $\Delta\alpha$, DF DL allows a measure of V_L . $\Delta\alpha$ depends on the optical frequency difference, α , but is independent of the laser optical frequency itself. The time-dependent portion of the signal in Eq. (13) is mathematically the same as if microwave energy of frequency α were being transmitted and Doppler-shifted to frequency $\alpha + \Delta\alpha$ before reception. The procedures for DF DL signal processing are, therefore, similar to those used in microwave Doppler radar.

The volume probed by a DF DL is defined by the optical layout. The transmitted beam, at most a few centimeters in diameter for adequate signal-to-noise ratio (SNR), specifies the transverse extent of the volume. The field of view of a bistatic receiver with optic axis intersecting the transmitted beam determines the range R and the volume length ΔR , with $R \gg \Delta R$. The scattering angle θ is within a few degrees of 180° , allowing the approximation $\theta = 180^\circ$ in Eq. (14) with little error.

The Doppler spectrum is broadened by the finite transit time of each particle through the volume. Let us adapt Eq. (13) to the geometry of the probed volume to obtain the detector output spectrum for one particle. Approximate θ as 180° and take $L_z = R$ in the denominator with little error, since $R \approx L_z \gg \Delta R$. For a Gaussian profile of each beam, the amplitude of beam #1 is given by

$$A_1^2 = (2A_{01}^2/\pi a^2) \exp[-2(x^2 + y^2)/a^2], \quad (15)$$

where the power in the beam is

$$P_1 = A_{01}^2, \quad (16)$$

and a is the e^{-2} radius. A similar expression holds for beam #2. If the intersecting angle between the beam and receiver axis is only a few degrees, $\Delta R \gg a$, in which case the transit time depends mainly on beam radius unless \vec{V} is nearly parallel to the beam. ΔR 's effect on transit time will be disregarded here, but can be included in a straightforward manner. The energy

spectrum, $W_i(\omega)$, for the Doppler signal portion of the detector current can be found by calculating the time-dependent current and using Fourier analysis. It has been demonstrated⁸ that the phase factor $\vec{k}_i \cdot \vec{R}_d$ in Eq. (13) is very nearly constant over an aperture area A_d of practical size. The time-varying signal current, therefore, has amplitude proportional to A_d . The spectrum is⁹

$$W_i(\omega) = \frac{4}{\pi} r^2 P_1 P_2 \frac{A_d^2}{R^4} \frac{\sigma_i^2}{(aV_T)^2} \exp\left[-\frac{4b_i^2}{a^2}\right] \exp\left[-\frac{(\omega - \alpha + 2KV_L)^2}{4V_T^2/a^2}\right], \quad (17)$$

where V_T is the component of particle velocity transverse to the beam, and b_i is the distance of closest approach to the beam axis. The detector's output also includes a low-frequency pulse arising out of the A_1^2 and A_2^2 terms of Eq. (13), but this part of the spectrum is neglected in Eq. (17) because it contains no Doppler information.

For atmospheric measurements, there will be, at any instant, a large number of scattering particles positioned throughout the probed volume. From Eq. (12), it can be seen that three types of signals will be included in the detector output. The terms of the first summation express the average irradiance at the detector of the light scattered from both beams by all the particles. These terms lead to DC output. The second summation is the information-bearing Doppler signal of DFDL, which is, for each particle, the beat frequency between the radiation scattered from the two beams. This yields a time-varying detector current, I_s . The terms in the double summation with $i \neq j$ arise from the mixing of radiation scattered from separate particles. This will be called the double-target signal, which produces a current I_{DT} . It can be shown⁹ that I_{DT} possesses negligible spectral energy within the final data-processing bandwidth, B , as a result of two factors. The double-target signal is reduced by the incoherent nature of its detection,

in a manner similar to that which occurs in the crossed-beam laser Doppler velocimeter.^{10,11} Also of primary importance⁹ is the fact that the spectrum of I_{DT} has a width much greater than B . The signal portion of the detector current for the Gaussian beam is, therefore,

$$I_s = \sum_i I_{si} , \quad (18)$$

$$I_{si} = \frac{2\pi}{R^2} \iint_{A_d} \sigma_i A_{1i}(t) A_{2i}(t) \cos(\omega t - \vec{k} \cdot \vec{R}_i - \vec{k}_i \cdot \vec{L}_i) dx dy , \quad (19)$$

where $A_{1i}(t)$ and $A_{2i}(t)$ depend on particle position in the beam.

If the particles are randomly positioned, the phases $\vec{k} \cdot \vec{R}_i + \vec{k}_i \cdot \vec{L}_i$ are also random, and the contributions of the particles to I_s then add in random-walk fashion. Thus,

$$\overline{I_s^2} = \sum_i \overline{I_{si}^2} , \quad (20)$$

and the expected value $W(\omega)$ of the energy spectrum of I_s is the sum of the spectra of the individual particles, or

$$W(\omega) = \sum_i W_i(\omega) . \quad (21)$$

This mean-square behavior has been established¹¹ for the corresponding case of dual-beam anemometry. The expected value of the power spectrum $P(\omega)$ of I_s is obtained by determining the rate of arrival of particles at the probed volume and integrating over the distribution $dn(\sigma)/d\sigma$ of scatter cross sections:

$$P(\omega) = \int_R^{R+\Delta R} dz \int_{-\infty}^{\infty} db \int_0^{\infty} d\sigma V_T W(\omega, \sigma, V_T, b) \frac{dn(\sigma)}{d\sigma} . \quad (22)$$

For the Gaussian beam profile:

$$P(\omega) = \frac{2}{\sqrt{\pi}} r^2 P_1 P_2 \frac{A_d^2 R}{R^4} \overline{n\sigma^2} \frac{1}{aV_T} \exp \left[- \frac{(\omega - \alpha + 2KV_L)^2}{4V_T^2/a^2} \right]. \quad (23)$$

The factor $\overline{n\sigma^2}$ is defined by

$$\overline{n\sigma^2} = \int_0^\infty \sigma^2 \frac{dn(\sigma)}{d\sigma} d\sigma = \int_0^\infty \sigma^2(\rho) \frac{dn(\rho)}{d\rho} d\rho, \quad (24)$$

where $dn(\rho)/d\rho$ is the particle size distribution over radius ρ , and n is the number density. The total signal power, P_s , is

$$P_s = 2r^2 \frac{P_1 P_2}{(\pi a^2)^2} \left[\frac{A_d}{R^2} \right]^2 \pi a^2 \Delta R \overline{n\sigma^2}. \quad (25)$$

In the atmosphere, aerosols dominate the factor $\overline{n\sigma^2}$, and the molecular contribution is negligible. For example, at optical wavelength $\lambda = 514.5$ nm, we have $n_m \overline{\sigma_m^2} = 1.3 \times 10^{-35}$ cm for a molecular density of $n_m = 2.6 \times 10^{19}$ cm⁻³ and molecular backscatter cross section of $\sigma_m = 7 \times 10^{-28}$ cm². For even a sparse distribution ($n_a = 10^{-6}$ cm⁻³) of small aerosols of radius 0.1 μ m with $\sigma_a = 7 \times 10^{-12}$ cm², the much larger value $n_a \overline{\sigma_a^2} = 5 \times 10^{-29}$ cm results. DFDL is unable to measure the distribution of molecular velocities and cannot succeed as a remote temperature sensor.

B. Signal-to-Noise Ratios

The wind component V_L must be acquired from the Doppler spectrum in the presence of noise originating during the photo-detection process. Of the principal noise sources for a photoemissive detector such as a PMT, the most significant for DFDL is shot noise from the scattered laser radiation and background light. In comparison, shot noise from dark current is negligible,

and thermal noise can be rendered insignificant by judicious choice of FMI gain. Shot noise power in bandwidth B is

$$P_N = 2q^2 p (\bar{I}_s + \bar{I}_b) , \quad (26)$$

where q is electronic charge, p is FMI current gain, and \bar{I}_s and \bar{I}_b are the average output currents resulting from scattered laser radiation and background light, respectively.

For the optical geometry used to derive $P(\omega)$, it is straightforward to show that

$$\bar{I}_s = p(P_1 + P_2) \frac{A_d}{R^2} \Delta\Omega \eta \bar{\sigma} , \quad (27)$$

where $\eta \bar{\sigma} = \bar{\sigma}_v$ is the volumetric angular-scatter cross section defined by

$$\eta \bar{\sigma} = \int_0^\infty \frac{d\eta(\omega)}{d\omega} d\omega = \int_0^\infty \sigma(\omega) \frac{d\eta(\omega)}{d\omega} d\omega , \quad (28)$$

which usually includes significant contributions from both molecules and aerosols. The detector responsivity is

$$r = \eta q \bar{\sigma} \Delta\Omega , \quad (29)$$

where η is quantum efficiency, and $\bar{\sigma}$ is the photon energy.

When shot noise from scattered laser radiation is the dominant noise source, the $\text{SNR} = P_s/P_N$ is

$$\text{SNR}_s = \frac{\eta}{2qB} \frac{P_1 P_2}{P_1 + P_2} \frac{1}{\pi R^2} \frac{A_d}{R^2} \frac{\bar{\sigma}^2}{\bar{\sigma}} . \quad (30)$$

When the background is of uniform radiance L ($\text{W m}^{-2} \text{sr}^{-1} \text{nm}^{-1}$), we have

$$\bar{I}_b = p \bar{\sigma}_b A_d \Delta\Omega , \quad (31)$$

where $\Delta\Omega$ is the optical passband, and $\bar{\sigma}_b$ the field of view in steradians.

If $\overline{I_b} \gg \overline{I_g}$, SNR becomes

$$\text{SNR}_b = \frac{\eta}{h\nu B} \frac{P_1 P_2}{(\pi a^2)^2} \frac{A_d}{R^4} \pi a^2 \Delta R \frac{\pi \sigma^2}{L \Omega_d \Delta \lambda}. \quad (32)$$

The functional dependence of P_g on various parameters appearing in Eq. (25) and in these SNR expressions was verified experimentally.⁹ The prototype DF DL described below was operated in a wind tunnel with flow seeded by a sparse mist of water droplets generated artificially. For each test, all experimental parameters were held constant except the variable under examination. The predicted behavior of P_g with changes in receiver collection solid angle A_d/R^2 , beam area $A_b = \pi a^2$, and scattering volume length ΔR was confirmed. The dependence of P_g on changes in laser power P_L , where $P_L = \frac{1}{2}P_1 = \frac{1}{2}P_2$, also agreed with Eq. (25).

C. Extraction of Velocity Information

$P(\omega)$ for the narrow Gaussian beam profile has a Gaussian shape with mean frequency $\alpha = 2KV_L$ and 1/e half-width $2\Gamma_p/\alpha$. In practice, this half-width can, at times, be comparable to, or even exceed, $\Delta\omega$. In such a case, V_L is obtainable from the power-weighted mean Doppler frequency $\bar{\omega}$, according to

$$V_L = \bar{\omega}/2K \quad (33)$$

$$\bar{\omega} = \frac{\int \omega P(\omega + \alpha) d\omega}{\int P(\omega + \alpha) d\omega}. \quad (34)$$

Several data-processing techniques for estimating $\bar{\omega}$ have been devised.¹²

Since the Doppler signal is generated by a random process, the Doppler spectrum undergoes random fluctuations about $P(\omega)$. Consequently, the mean Doppler frequency, $\bar{\omega}$, is a random variable with statistical perturbations about its expected value. The shot-noise spectrum is also random and

contributes to the fluctuations in $\bar{\omega}$ even when the average noise level is known. Since the DFOL Doppler signal is mathematically like that of the scattering of microwaves of frequency ω from the particles, the DFOL statistics are the same as for Doppler radar returns from randomly positioned hydrometeors. A detailed consideration^{9,12} of the statistical variations in $\bar{\omega}$ shows that they figure prominently in limiting the accuracy to which V_z can be determined.

D. Hybrid DFOL

A hybrid DFOL is created if the two transmitted beams are not exactly superimposed but intersect with \hat{k}_1 and \hat{k}_2 separated in direction by a small angle. The descriptor "hybrid" is applied because this configuration combines features of DFOL with the dual-beam (or crossed-beam) Doppler anemometer.⁹

In Fig. 2, the wave vectors \hat{k}_1 and \hat{k}_2 of two transmitted beams both lie in the $x - z$ plane at equal angles $\theta/2$ from the z -axis. Scattered radiation is detected at \hat{K}_d a large distance away ($K_d \gg K_t$). The radiation incident on a particle is

$$E_{\text{inc}} = A_1 \cos(\omega_1 t - \hat{k}_1 \cdot \hat{R}_p) + A_2 \cos(\omega_2 t - \hat{k}_2 \cdot \hat{R}_p). \quad (35)$$

The beams interfere spatially, as well as temporally, to form fringes which travel at speed c in the z -direction, but which are oriented at an oblique angle.

Assuming, as before, that $\hat{K}_t = \hat{K}_{dt} + \hat{V}_t t$, $\hat{K}_d = \hat{K}_{dt} + \hat{V}_d t$, and that particle speeds are nonrelativistic, the scattered radiation at \hat{K}_d from one particle is

$$E_d = (R_d/R_t)^2 \{ A_1 \cos[\omega_1 t - (\hat{K}_1 - \hat{K}_{dt}) \cdot \hat{V}_t t - \phi_{1t}] + A_2 \cos[\omega_2 t - (\hat{K}_2 - \hat{K}_{dt}) \cdot \hat{V}_t t - \phi_{2t}] \} \quad (36)$$

where ϕ_{1i} and ϕ_{2i} are phases determined by particle position at $t = 0$. As discussed earlier, the spectrum of the information-bearing portion of the signal for multiple particles at random positions is the sum of the spectra of the individual particles. The double-target signal also exists but again is negligible. The signal from one particle is therefore sufficient to describe the behavior of a hybrid DFOL. For one particle, the detector current is

$$I_i = \frac{\pi A_d \sigma_i}{L_i^2} (A_1^2 + A_2^2) + \frac{2\pi A_d \sigma_i}{L_i^2} A_1 A_2 \cos[\alpha t - (\vec{k}_1 - \vec{k}_2 - \vec{k}_{1i} + \vec{k}_{2i}) \cdot \vec{V}_i t - \phi_{1i} + \phi_{2i}]. \quad (37)$$

The differential Doppler shift, $\Delta\alpha$, involving the dot product of \vec{V}_i with the wave vectors is

$$\Delta\alpha = (\alpha/c) \vec{V} \cdot (\vec{L}/L) - [(v_1 + v_2)/c] \sin(\phi/2) V_x - (\alpha/c) \cos(\phi/2) V_z, \quad (38)$$

where the i subscripts have been dropped and V_x (V_z) is the x -component (z -component) of \vec{V} . Taking $\phi \ll \pi/2$ and $v_1 + v_2 = 2v_0$, the Doppler shift is

$$\Delta\alpha = -2(v_0/c) \sin(\phi/2) V_x - 2(\alpha/c) \sin(\theta/2) V_b, \quad (39)$$

where V_b is the velocity component along the bisector of \vec{L} and the negative z -axis.

Two limiting cases are immediately identifiable. If $\phi = 0$ but $\alpha \neq 0$, we have the pure DFOL arrangement

$$\Delta\alpha_{\text{DFOL}} = -2(\alpha/c) \sin(\theta/2) V_b. \quad (40)$$

The dual-beam anemometer (DBA) occurs in the opposite case when $\phi \neq 0$ and $\alpha = 0$, giving

$$\Delta\alpha_{DBA} = -2(v_0/c) \sin(\phi/2) V_x. \quad (41)$$

The detector beat frequency for hybrid DF DL can be expressed as

$$\omega = \alpha + \Delta\alpha_{DFDL} + \Delta\alpha_{DBA}, \quad (42)$$

In which both α_{DFDL} and α_{DBA} are significant.

For the case of backscatter, the hybrid DF DL has differential frequency shift

$$\Delta\alpha = \vec{K}_h \cdot \vec{V}, \quad (43)$$

$$\vec{K}_h = -(2/c)[v_0 \sin(\phi/2) \hat{z} + \alpha \hat{k}]. \quad (44)$$

The component of velocity measured lies in the x - z plane, parallel to \vec{K}_h .

The angle β of this component from the z -axis is, from Eq. (44),

$$\beta = \tan^{-1} [v_0 \sin(\phi/2)/\alpha]. \quad (45)$$

The Doppler frequency sensitivity is given by

$$\Delta\alpha = (2/c)[v_0^2 \sin^2(\phi/2) + \alpha^2]^{1/2} V_h = K_h V_h, \quad (46)$$

where V_h is the component of \vec{V} parallel to \vec{K}_h . The hybrid DF DL can measure an arbitrary component of velocity selected by the choice of optical frequencies v_1 and v_2 and the intersection angle ϕ .

Usually in dual-beam anemometers, the beams are spatially distinct at the transmitter and converge to a common volume. This may not be true for the hybrid DF DL, whose intersection angle might be less than a laser beam's divergence angle. For instance, if $\lambda_0 = 514.5$ nm, $\alpha/2\pi = 10^9$ s⁻¹, and $\beta = 45^\circ$, the required value of ϕ from Eq. (45) is only 3.4×10^{-6} rad.

SNR expressions for hybrid DF DL are similar to those for pure DF DL. The effect of partially overlapping beams in the probed volume is accounted for through the amplitude factors $A_1(\vec{R})$ and $A_2(\vec{R})$. In the vicinity of the

Intersection of the beam axes, the hybrid SNR is the same as for pure DFOL with proper allowance in bandwidth B for the increased Doppler sensitivity.

III. Prototype DFOL

A DFOL system was assembled to experimentally evaluate this technique of wind sensing. It is capable of real-time measurement and recording of wind and can operate in pure or hybrid DFOL modes. In accordance with the research nature of this study, the range capability of the prototype is modest, but it can be markedly increased within the limits of existing technology.

A brief description of the system, shown schematically in Fig. 3, is presented here, with a comprehensive treatment available elsewhere.⁹ The Spectra Physics Model 166-03 argon laser operates at frequency ν_0 ($\lambda = 514.5$ nm), with a cavity dumper, Model 365 Acousto-Optic Output Coupler, producing the exiting beam. This coupler acts as a modulator, creating two overlapping beams of respective frequencies $\nu_1 = \nu_0 + \alpha/2$ and $\nu_2 = \nu_0 - \alpha/2$. The desired pure or hybrid DFOL configuration is selected by adjustment of the acousto-optic modulator's position within the laser cavity. The RF oscillator generates the system reference frequency, which is amplified to drive the modulator. The transmitting optics consist of an appropriate beam expander and steering mirrors. Light scattered and Doppler-shifted by aerosols moving with the air is collected by a telescope and passed through a 30 \AA passband interference filter for reduction of background light. The high-speed FMT, which must be capable of electronic response at the modulation frequency α , was manufactured by Varian LSE and is specified to have a $0 - 3$ db bandwidth of approximately 10^3 to 10^6 Hz. The output of the FMT is separated from the high-frequency signal and monitored. The high-frequency portion proceeds to the microwave Doppler receiver, which performs signal amplification and

heterodyne mixing with an offset local oscillator of frequency $\alpha + \xi$. This frequency is developed from the output frequencies of the RF oscillator and an audio-frequency oscillator. For $V_L = 0$, the Doppler spectrum is thus displaced from $\Delta\alpha = 0$ to $\Delta\alpha = \xi$, which removes the directional ambiguity in the velocity measurement. A real-time spectrum analyzer, Princeton Applied Research Model 4512, digitizes the signal and computes the Fourier amplitude spectrum. A PDP11V03 minicomputer computes V_L and other information of interest from the spectrum, stores this data on floppy disk, and displays it on the computer console.

The optical frequency difference is $\alpha/2\pi = 970$ MHz, which gives a frequency sensitivity for a pure DFBL operating in backscatter of $\Delta\alpha/2\pi = 6.47$ Hz for $V_L = 1$ ms⁻¹. The mean Doppler frequency is obtained with the fast Fourier transform technique with noise suppression (FFT, NS).¹¹ Since the shot-noise level can vary in time, the average noise level for each velocity sample is determined over a frequency band separated from the Doppler spectrum. This value is then subtracted from the combined spectrum of Doppler signal plus shot noise, to remove the biasing effects of the average noise level. From the resulting Doppler spectrum, and with proper allowance for the offset ξ , the mean Doppler frequency is calculated according to eq. (34). V_L or V_H are found using Eq. (33) or (46), as the case may be.

The prototype DFBL can also be operated as a pulsed system when the cavity dumper (i.e., modulator) is driven by a pulsed amplifier. The receiver can be range gated, which (for coaxial transmitter and receiver optics) defines the range R and probed volume length Δz . By converting to such a pulsed system, the SNR can be improved when shot noise from background light is substantial, on condition that the average transmitted laser power is maintained.

In order to accomplish this with the present equipment, a high pulse rate (21 MHz) is necessary. The low-pass filter characteristics of the Doppler receiver transform the signal from a pulsed to a continuous form, and no other changes in the data-processing procedures are needed.

The prototype DFDL was operated CW in a laboratory setting, using targets undergoing controlled motion. These experiments,⁹ together with the wind measurements reported here, have verified the differential Doppler shift, which is the fundamental principle of DFDL.

IV. Wind Measurements

A component of wind velocity was successfully measured with the DFDL in various configurations: pure and hybrid, pulsed and CW. The DFDL equipment (see Fig. 3) was located in a penthouse atop the five-story Physics-Atmospheric Sciences Building on the University of Arizona campus. The dual-frequency beam from the laser was expanded and collimated to an e^{-2} diameter of approximately 2.5 cm and then projected through an open window. For the measurements described in detail here, the beam was horizontal at a height of 4.3 m above the main roof. The range $R = 20$ m and length $\Delta R = 2.2$ m of the probed volume were defined by the intersection of the beam with the field of view of the Newtonian receiving telescope, which has a 41-cm diameter primary. Since the tops of the surrounding buildings and trees were at the same general level as the probed volume, the air flow was usually quite turbulent. A propellor anemometer, Weather-Measure Model W173B, was positioned with the hub about 20 cm from the center of the probed volume. It was aligned to measure the same component of wind for which the lidar was set. For example, for alignment angle $\beta = 0$, the westerly component parallel to the beam was obtained. A wall (not shown) at a distance of 41 m acted as a beam stop. A light trap, consisting of a

box with a black interior with an open side facing the telescope, was mounted on the wall to encompass the receiver's field of view. The trap was required to prevent background light from the sunlit wall from saturating the PMT, which had considerably higher gain than anticipated when purchased. The trap also diminished the shot noise caused by background light. In order to further reduce this shot noise, the laser output was pulsed and the Doppler receiver range gated. Since the pulse length was 15 ns and the receiver gate time was 30 - 40 ns, the probed volume was still defined mainly by the intersection of the beam with the field of view. Pulse repetition rates were typically 3.5 MHz, which gave a receiver duty factor of roughly 12%.

Figure 5 shows the time series of wind velocity from the lidar and anemometer plotted side by side for an example data run. The similar response of the two methods to velocity fluctuations is apparent. The anemometer's trace is smoother than the lidar's because the statistical nature of the Doppler and shot-noise spectra inject random fluctuations into the Doppler velocity. The experimental particulars for this data run and three others are given in Table I. Wind measurements at several values of the alignment angle β ($= 0^\circ$ for pure DF DL, $\neq 0^\circ$ for hybrid) were made. Average transmitted laser power was 1/3 W. The sampling rate was slightly slower than $1/T$, where T is the signal-averaging time for each velocity sample.

Table I also shows, for each of these data runs, the individual and comparative statistics of the anemometer velocity V_A and the Doppler velocity V_D . The agreement between the two methods is satisfactory, although differences do exist. A small bias is revealed by $\overline{V_D}/\overline{V_A} < 1$. A linear regression slope of less than unity, combined with the intercept displaced slightly toward $\overline{V_A}$, also points out the bias. The rms difference

Table I. Summary of Selected Wind Data Runs

Date	March 7	March 19	April 4	April 4
Starting time	1713	1402	1407	1901
<u>Equipment Parameters</u>				
Alignment angle β	63°	-45°	0°	83°
Laser average power (W)	.36	.36	.31	.36
Sample averaging time T (s)	2.0	1.0	1.5	1.0
Length of data run (min)	30	27	10	24
<u>Wind Statistics</u>				
Average anemometer velocity $\overline{V_A}$ (ms^{-1})	4.28	-2.23	1.28	2.14
Average Doppler velocity $\overline{V_D}$ (ms^{-1})	4.09	-2.07	1.12	2.10
Standard deviation of V_A (ms^{-1})	1.80	1.26	1.04	1.17
Standard deviation of V_D (ms^{-1})	1.85	1.21	1.08	1.03
$\overline{V_D}/\overline{V_A}$.96	.93	.88	.98
$[(V_D - V_A)^2]^{\frac{1}{2}}$.79	.61	.58	.46
<u>Linear Regression Analysis ($V_A=x, V_D=y$)</u>				
Slope	.937 \pm .016	.855 \pm .012	.897 \pm .028	.812 \pm .011
y-intercept (ms^{-1})	.08 \pm .08	-.16 \pm .03	-.02 \pm .03	.36 \pm .03
Correlation coefficient	.91	.89	.86	.92
<u>Signal-to-Noise Ratio Statistics</u>				
Bandwidth B (Hz)	797	401	301	785
Average SNR	1.80	3.96	3.71	1.91
Standard deviation of SNR	1.10	2.69	2.87	3.15
<u>Aerosol Optical Properties</u>				
Aerosol backscatter cross section β_a ($\times 10^{-6} m^{-1} sr^{-1}$)	—	.43 \pm .20	.95 \pm .26	.63 \pm .22
$\overline{\sigma_a^2}/\sigma_a$ ($\times 10^{-12} m^2 sr^{-1}$)	—	3.8 \pm 1.9	2.5 \pm 1.3	2.2 \pm 1.1

between V_D and V_A results from a combination of biased and unbiased discrepancies. The disagreement is caused by imperfections in both methods. Based on manufacturer's data, the anemometer is calibrated for axial flow at 2.2 ms^{-1} . For somewhat slower axial flow, it indicates an excessive value for V_A (17% too high at $.45 \text{ ms}^{-1}$), while the threshold speed is 0.5 ms^{-1} . For wind at large yaw angles, the response does not exactly follow the cosine of the yaw angle, and V_A tends toward values which are too small. In the case of high wind speeds, the DF DL measurement is biased toward small values because the tail of the Doppler spectrum falls outside the final data-processing bandwidth. Refinements in the data processing can be expected to diminish this particular source of error. The observed bias between V_D and V_A is compatible with the features of the individual instruments. The major portion of the rms difference is caused by the random variations introduced into V_D by the statistical nature of the Doppler and shot-noise spectra. Because of these random variations in V_D , we would expect its standard deviation to exceed that of V_A , but the data show otherwise. A reasonable explanation is that, as mentioned, the DF DL data processing diminished V_D for high wind speeds, which would also decrease V_D 's standard deviation. Other sources of error of less importance were also present. They include the inaccuracy in setting the DF DL to measure the desired component of velocity at angle β , the lag time in the propeller anemometer, and the physical separation of the anemometer from the DF DL-probed volume.

The values of SNR were rather small. They could have been increased by narrowing the probing beam, but accuracy in V_D would have improved by less than 30% because the Doppler spectrum would have been correspondingly broadened.

The aerosol volumetric backscatter cross section β_a and the aerosol optical characteristic $\overline{\sigma_a^2}/\overline{\sigma_a}$, which is important to DFDL SNR, were measured with the lidar. $\overline{\sigma_a}$ is the average aerosol backscatter cross section, and $\overline{\sigma_a^2}$ is the mean square average. β_a for $\lambda = 514.5$ nm was determined by measuring the total atmospheric backscatter cross section before or after a wind-data run and subtracting the molecular contribution $\beta_m = 1.6 \times 10^{-6} \text{ m}^{-1} \text{ sr}^{-1}$ calculated for the ambient air pressure and temperature. The low β_a values imply very clean air, a fact corroborated by a visual range exceeding 50 miles. The factor $\overline{\sigma_a^2}/\overline{\sigma_a}$ was obtained by solving the SNR expression in Eq. (30) for it and calculating its value from the experimentally determined SNR, known equipment parameters, and data on the energy received from molecular scatter, aerosol scatter, and background light. The details are too extensive to give here but can be found elsewhere.⁹ Aerosol size distributions were also measured with a Climet optical particle counter. This collection⁹ of data on the aerosols acting as tracer targets is valuable in predicting the performance of DFDL under different aerosol conditions.

Although not described in detail here, wind measurements were also accomplished in the bistatic optical arrangement shown in Fig. 3 with the transmitter and receiver operated CW. Successful operation was also achieved in a fully pulsed configuration, in which the transmitting and receiving optics were coaxial, and the probed volume at $R = 20$ m and $\Delta R = 4.2$ m was defined by pulsing the laser and range-gating the receiver.

V. Projected Capabilities

An estimate of the range capability of an upgraded system can be made, based on the performance of the prototype DFDL (20 m range) and the scaling factors in SNR. Since P_1 and P_2 are both proportional to laser power P_L ,

Eq. (30) shows $\text{SNR} \propto P_L$. Boosting the transmitted laser power from 1/3 to 10 W would increase the range capability for the same SNR by a factor of 5.5. Substantial improvements in the PMT's high-frequency response and quantum efficiency are also within the realm of existing technology¹³ and could extend range capability by almost a factor of 2. Range and/or accuracy could also be increased if the sample-averaging time were lengthened or a larger telescope used. Enhancement of DF DL performance can also be achieved with a higher modulation frequency α . By scaling the beam radius inversely with α , and the bandwidth B proportional to α , the range capability scales as $\sqrt{\alpha}$ for constant SNR. Better accuracy is an additional benefit, for the fractional error in V_D due to statistical fluctuations in the spectrum scales under these conditions as $1/\sqrt{\alpha}$.⁹

Adequate reduction of shot noise from the background light is a critical factor for daytime operation. A narrowband interference filter in the receiving optics is essential, but it may not bring the transmitted light level so low as to make the SNR limited by scattered laser radiation. The best solution might be a pulsed DF DL with small receiver duty factor, in which the light scattered from the high-power pulse would dominate the background light while the receiver is gated open. The pulse-repetition frequency must satisfy the Nyquist frequency criterion for the baseband data-processing bandwidth B .

Although the FFT/NS technique was ideal for data processing during this experimental study, it may not be the optimum method for an operational wind-sensing system. Burst-signal processing is superior to continuous processing in the dual-beam anemometer⁴ and would probably be likewise advantageous in DF DL. Pulse-pair processing is also superior to FFT/NS in some respects, especially for low SNR.¹²

An important asset⁹ of DF DL is its resilience to the effects of degradation of laser beam coherence caused by atmospheric scintillations. Since, at least for the pure DF DL, the two transmitted beams are superimposed and are of nearly identical frequency, inhomogeneities in the atmosphere's index of refraction perturb the beams in nearly identical manner, and the amplitudes as well as the phases of the two beams remain highly correlated.^{14,15} The traveling fringe pattern of the DF DL beam thus remains well-defined, although substantial intensity variations across the beam can develop. The velocity information in the mean Doppler frequency remains fully available, although the shape of the Doppler spectrum, which depends mainly on the beam profile and the transverse speed of the tracer particle, is modified. In conjunction with this topic, it should be noted that, after the dual-frequency beam is formed, diffraction-limited optics are unnecessary, although they are desirable in the transmitter to maintain a smooth beam profile.

The novel ability of the hybrid DF DL to measure the velocity component parallel to a selectable skew direction is perhaps the most intriguing feature of this instrument. In principle, the hybrid DF DL concept could be incorporated into a device to measure three-dimensional velocity within a common probed volume from a single transmitter-receiver site. Multiple hybrid DF DL beams of different fringe orientations could be simultaneously transmitted with polarization, wavelength, or other technique to discriminate among the beams. It may also be possible to combine the DF DL concept with the time-of-flight laser anemometer. Two beams transmitted side by side would yield at low frequency the time of flight of the dust particles, which is a measure of transverse wind velocity. If the beams were both modulated as in pure DF DL, the differential Doppler spectrum carrying the information for the

longitudinal component of velocity would be simultaneously available near the modulation frequency α . Of course, the shape of the Doppler spectrum would be a function of the bifurcated beam profile.

VI. Summary

This research has demonstrated that a component of wind speed can be remotely measured with the DF DL technique using naturally existing aerosols as tracers of air motion. If the probing beams of different frequency are coaxially aligned (pure DF DL), the velocity component parallel to the beams is measured when the detector is positioned to receive backscattered radiation. If the beams intersect at a very small angle ($< 10^{-5}$ rad in the prototype instrument), this hybrid mode of DF DL determines a component in a skew direction, which is a function of the optical frequencies and the intersection angle. The velocity information is available from the mean frequency of the differential Doppler spectrum. The prototype DF DL performed satisfactorily in laboratory tests and in actual wind measurements. In harmony with its experimental nature, the prototype's capability (20 m range with a typical sampling rate of 0.7 Hz) was modest but can be improved more than an order of magnitude within the limits of existing technology. Expressions for SNR and auxiliary data on the optical characteristics of the aerosols allow extrapolation of the performance of an upgraded instrument.

DF DL possesses several advantageous features. It measures a different component of velocity than the dual-beam Doppler anemometer⁴ or time-of-flight laser anemometer,⁵ which also operate best at visible wavelengths. The three-dimensional wind could, in principle, be measured with a multiplexed hybrid DF DL, or with DF DL in combination with the time-of-flight anemometer. The DF DL should be capable of functioning through an atmosphere

rendered optically imperfect by turbulence-generated density inhomogeneities. Since the raw signal from the photodetector is similar to that of microwave Doppler radar, the data-processing procedures for estimating the Doppler velocity can utilize the optimal analysis methods which have been developed for radar.¹² The sense of direction of the wind is made unambiguous in DFDL in a straightforward manner, by offsetting the reference frequency in the receiver electronics.

An optimum DFDL system would utilize a laser emitting high average power in the visible, in order to maximize SNR. The modulation frequency, *i.e.*, the difference in the optical frequencies of the probing beams, would preferably be as high as can be produced and detected. For reduction of shot noise due to daytime background light, a pulsed DFDL system with a small receiver duty factor plus an interference filter would be ideal.

The authors thank M. Sanderson Rae for editing the final manuscript. Financial support was provided by National Science Foundation grant DES 74-22630 and by grants DAAG 29-76-G-0115 and DAAG 29-75-G-0026 of the Army Research Office.

References

1. T. R. Lawrence *et al.*, Rev. Sci. Instr. **43**, 512 (1972).
2. M. J. Post *et al.*, J. Appl. Meteor. **17**, 1179 (1978).
3. G. Benedetti-Michelangeli, F. Congeduti, and G. Flocco, J. Atmos. Sci. **29**, 906 (1972).
4. K. G. Bartlett and C. Y. She, Appl. Opt. **15**, 1980 (1976).
5. L. Lading *et al.*, Appl. Opt. **17**, 1486 (1978).
6. R. L. Armstrong, J. B. Mason, and T. Barber, Appl. Opt. **15**, 2891 (1976).
7. E. W. Eloranta, J. M. King, and J. A. Weinman, J. Appl. Meteor. **14**, 1485 (1975).
8. R. M. Schotland, "Optical Probing of the Atmosphere, Final Report," U. S. Army Electronics Command R&D Tech. Rpt. ECOM-0201-F, Fort Monmouth, N.J. (1972).
9. W. L. Eberhard, Ph.D. Dissertation, University of Arizona (1979).
10. C. Y. She and L. S. Wall, J. Opt. Soc. Am. **65**, 69 (1975).
11. L. E. Drain, J. Phys. D: Appl. Phys. **5**, 481 (1972).
12. D. Sirmans and B. Bumgarner, J. Appl. Meteor. **14**, 991 (1975).
13. H. Melchior, M. B. Fisher, and F. R. Arams, Proc. IEEE **58**, 1466 (1970).
14. P. A. Mandics *et al.*, Radio Sci. **9**, 723 (1974).
15. A. G. Kjelaas, P. E. Nordal, and A. Bjerkestrand, Appl. Opt. **17**, 277 (1978).

Figure Legends

- Figure 1 Geometry for derivation of pure DF DL signal.
- Figure 2 Geometry for derivation of hybrid DF DL signal.
- Figure 3 Equipment schematic of DF DL prototype.
- Figure 4 Optical layout for wind measurements with the probed volume defined by the intersection of the beam and receiver field of view.
- Figure 5 Velocity data commencing at 1713 on March 7. The upper trace gives the velocity from the lidar, while the lower one is from the propellor anemometer. The arrows indicate the appropriate velocity scales, which are displaced 5 ms^{-1} .

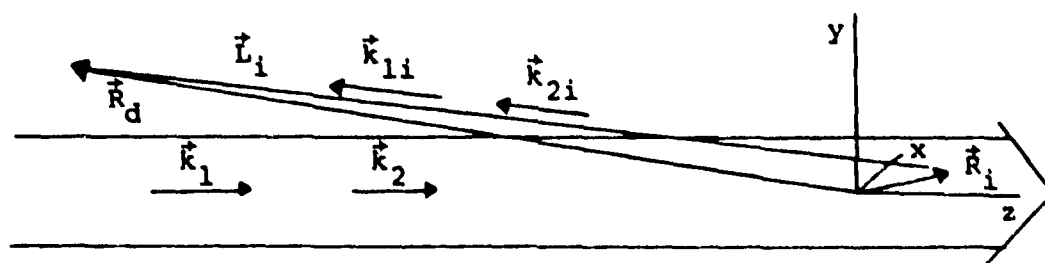


Fig. 1 Geometry for derivation of pure DFDL signal.

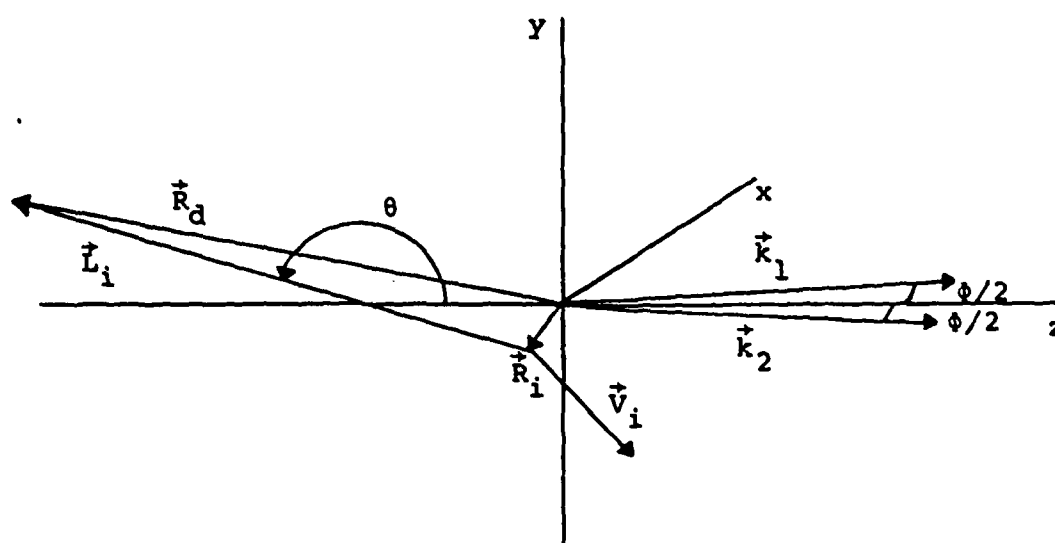


Fig. 2 Geometry for derivation of hybrid DFDL signal

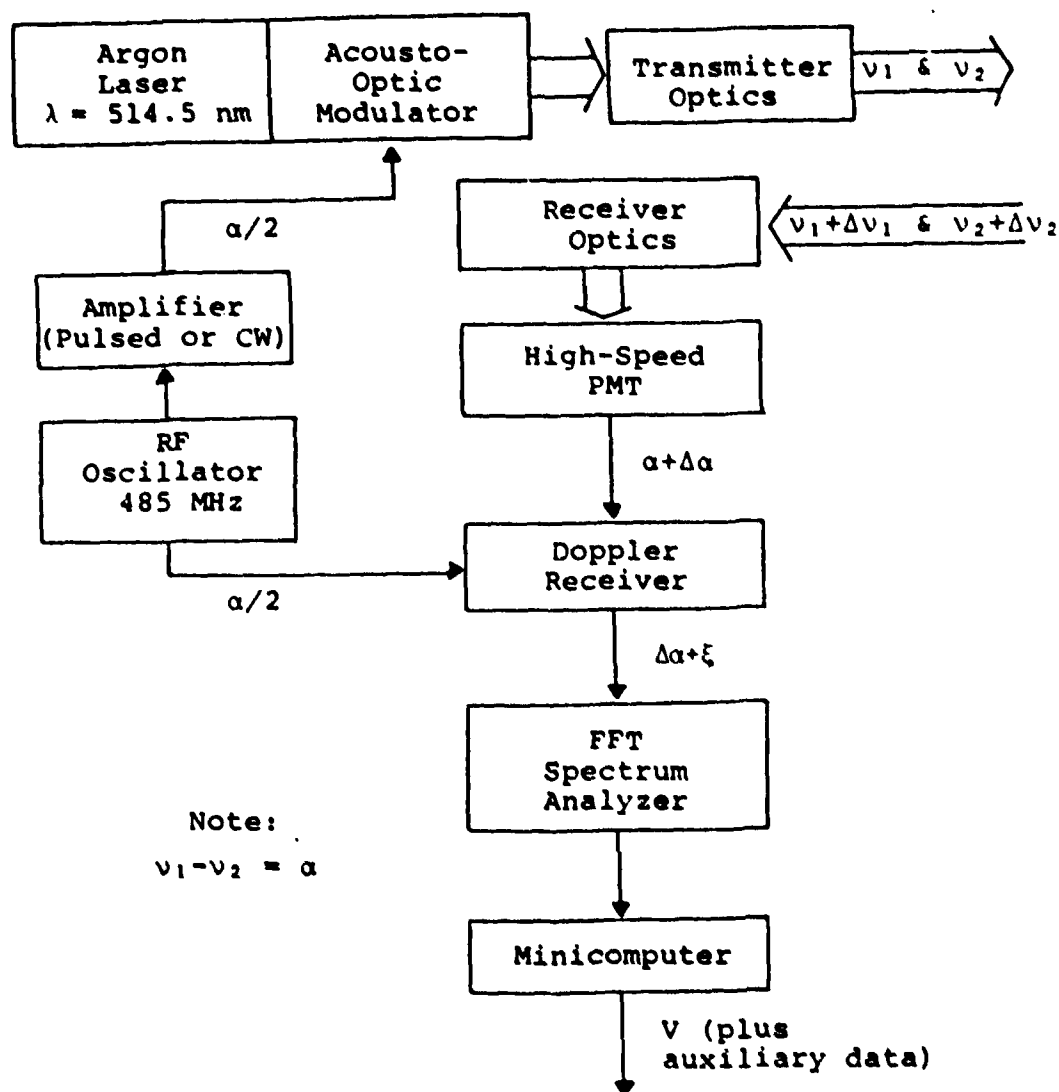


Fig. 3 Equipment schematic of EPDL prototype.

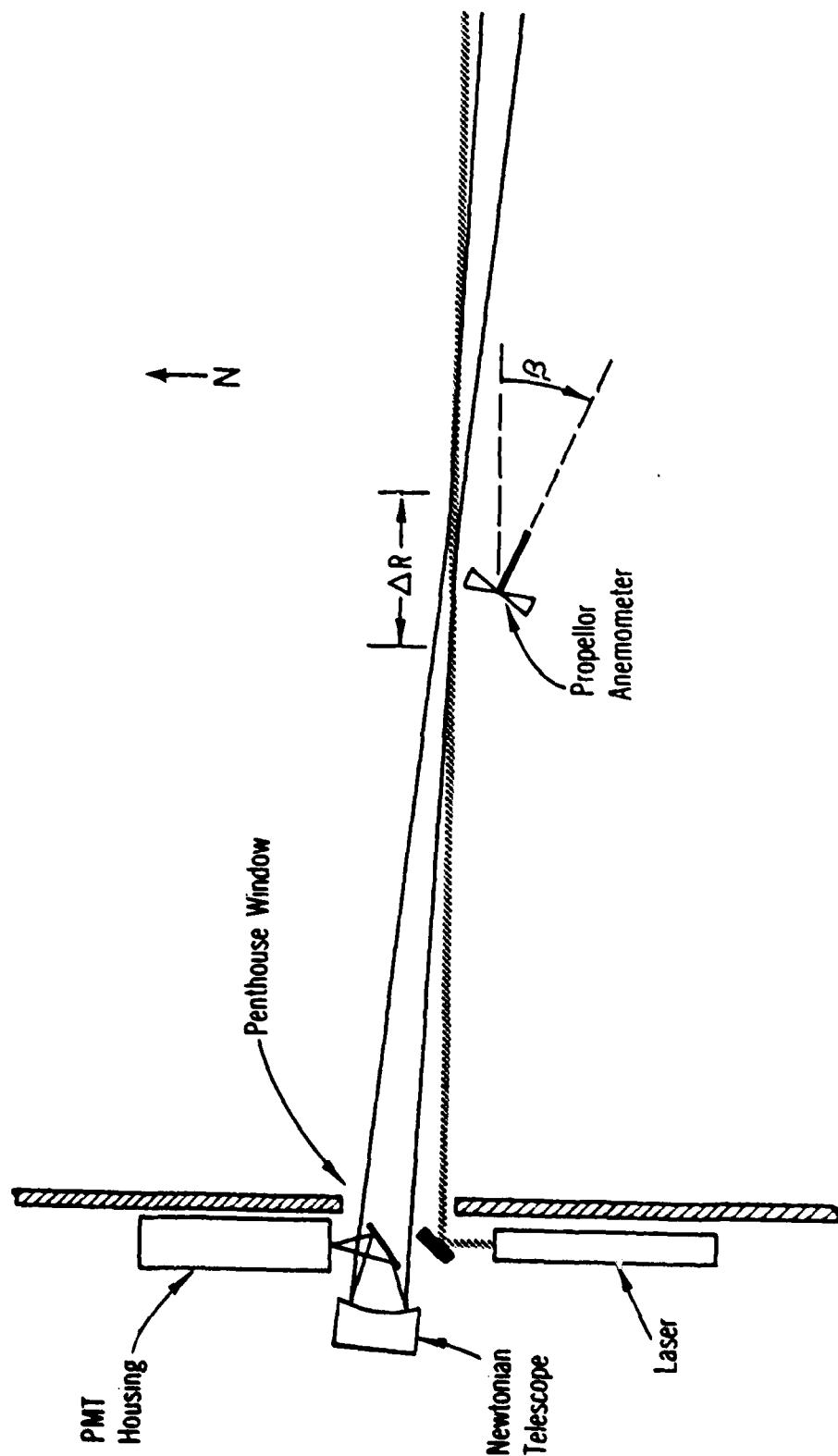
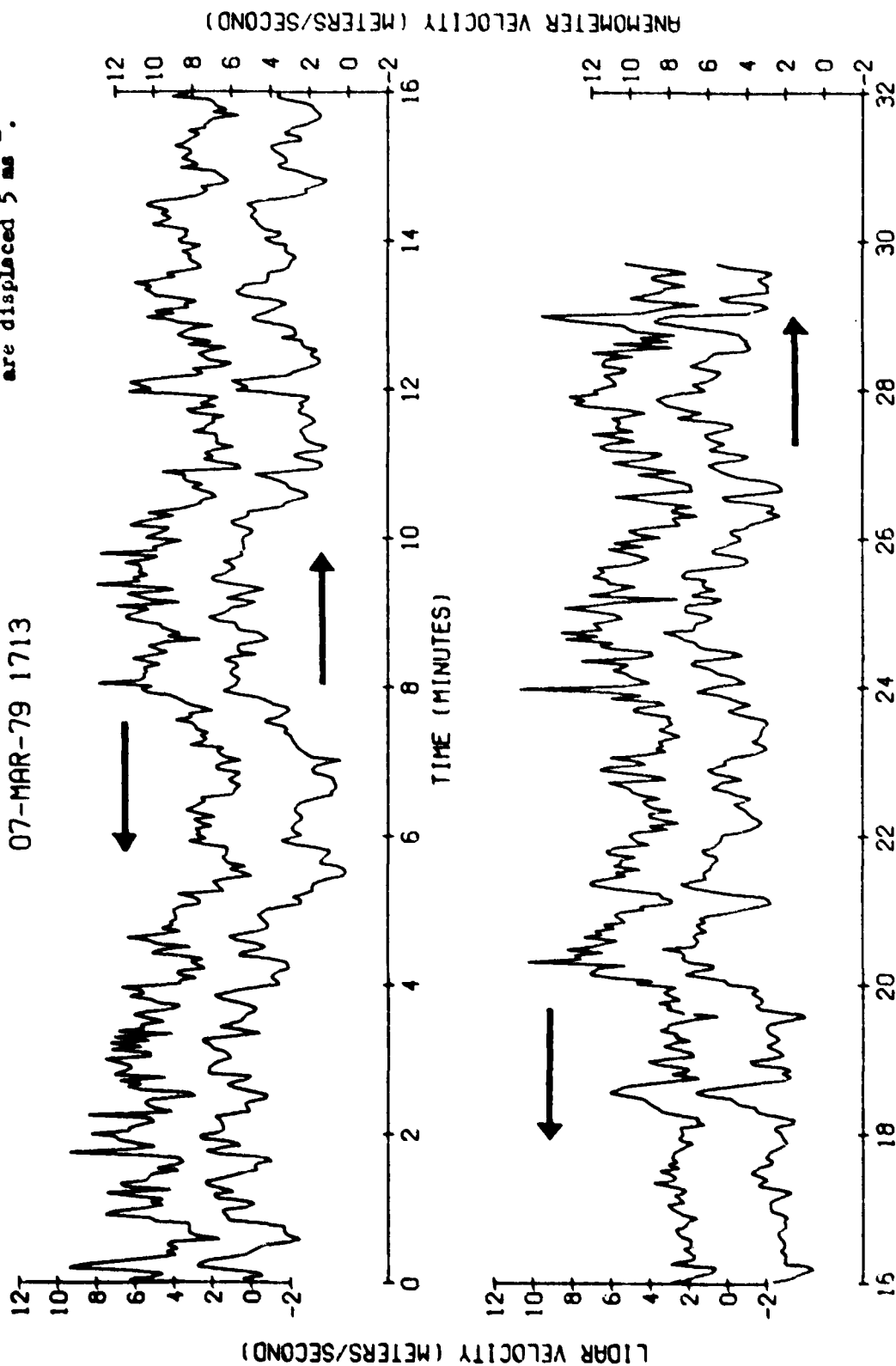


Fig. 4 Optical layout for wind measurements with the probed volume defined by the intersection of the beam and receiver field of view

Fig. 5 Velocity data commencing at 1713 on March 7. The upper trace gives the velocity from the lidar, while the lower one is from the propeller anemometer. The arrows indicate the appropriate velocity scales, which are displaced 5 m s⁻¹.

07-MAR-79 1713



LIST OF MANUSCRIPTS SUBMITTED OR PUBLISHED UNDER ARO SPONSORSHIP

"Wind Speed Measurement with a Dual-Frequency Doppler Lidar"
presented at Dynamic Flow Conference, Baltimore, September
18-21, 1978.

"The Dual-Frequency Doppler Lidar Technique for Wind Measurement"
presented at Ninth International Laser Radar Conference on Laser
Atmospheric Studies, July 2-5, 1979, Munich, Germany.

"Dual Frequency Doppler-Lidar Method of Wind Measurement"
submitted to Applied Optics.

SCIENTIFIC PERSONNEL SUPPORTED BY THIS PROJECT AND DEGREES
AWARDED

Richard M. Schotland, Principal Investigator

Wynn L. Eberhard, Graduate Associate in Research

Ph.D. degree awarded to Wynn L. Eberhard October 1979.
Dissertation Title: "Design and Performance of an Experimental
Dual-Frequency Doppler Lidar for Remote Measurement of Wind
Velocity".